

Robust Design of Connected Cruise Control Among Human-Driven Vehicles

Dávid Hajdu¹, Jin I. Ge², Tamás Insperger¹, and Gábor Orosz

Abstract—This paper presents the robustness analysis for the head-to-tail string stability of connected cruise controllers that utilize motion information of human-driven vehicles ahead. In particular, we consider uncertainties arising from the feedback gains and reaction time delays of the human drivers. We utilize the linear fractional transformation and the M- Δ uncertain interconnection structure to represent the uncertainties in the block-diagonal matrix Δ . The uncertain gains are directly incorporated in the uncertain interconnection structure, while the uncertain time delays are taken into account using the Rekasius substitution that preserves the tightness of the robustness bounds. This modeling framework scales well for large-size connected vehicle systems. We demonstrate through two case studies how parameters in the connected cruise controller can be selected to ensure the robust string stability. Theoretical results are supported by the experiments that highlight the advantage of robust control designs.

Index Terms—Connected vehicles, robustness, structured singular values.

I. INTRODUCTION

OVER the past few decades, passenger vehicles are equipped with more and more automation features in order to improve active safety, passenger comfort, and traffic efficiency of the road transportation system. In particular, adaptive cruise control (ACC) was invented to automate the longitudinal dynamics and alleviate human drivers from the constant burden of speed control [1]. While the influence of ACC is yet to be observed in real traffic due to its low penetration rate, theoretical studies have found that automated vehicles may have limited benefits on traffic flow [2], [3]. In particular, ACC vehicles may not be able to effectively

suppress the speed fluctuations propagating through the vehicle string, as each vehicle only responds to its immediate predecessor [4].

In order to overcome such limitations in an automated vehicle platoon, cooperative adaptive cruise control (CACC) was proposed using vehicle-to-vehicle (V2V) communication [5]–[8]. CACC has been shown to improve fuel economy and traffic efficiency in both theoretical and experimental studies [9]–[12]. However, the application of CACC in the early stages of driving automation may be significantly limited by the requirement that all vehicles in a CACC platoon must be automated aside from being equipped with vehicle-to-everything (V2X) communication devices [13], [14]. In particular, as mentioned in [15], “at low market penetrations, . . . the probability of consecutive vehicles being equipped is negligible”. Given the relatively low cost of V2X devices compared with ACC and other driving automation systems, it is desirable to exploit the benefits of V2X without being restricted by the penetration rate of automation. Thus, we need to consider a connected automated vehicle design that is able to utilize V2X information sent from human-driven vehicles ahead.

For the longitudinal control of such a connected automated vehicle design, we proposed a class of connected cruise controllers (CCC) that exploit ad-hoc V2X communication with multiple human-driven vehicles ahead [16]. By utilizing motion information from multiple vehicles ahead, connected cruise control is able to gain “phase lead” as it responds to speed fluctuations propagating along the vehicle chain [17]. Several theoretical studies have shown that connected cruise control is able to significantly improve active safety, fuel economy, and traffic efficiency of the connected automated vehicle, especially by providing head-to-tail string stability [18]–[21].

Safety, stability and efficiency are important requirements that the automated vehicle must meet even in case of partially known vehicle parameters and external disturbances. Since connected automated vehicle design relies on models, uncertainties need to be considered to guarantee robust performance of the connected vehicle system. In order to guarantee robust performance, \mathcal{H}_∞ framework was often used to synthesize controllers. For example, an \mathcal{H}_∞ -controller for a discrete time system with Markovian jumping parameters was introduced by [22], a centralized controller design using a mixed $\mathcal{H}_2/\mathcal{H}_\infty$ method was used in [23], while a decentralized solution without a designated platoon leader was presented in [10].

Manuscript received April 30, 2018; revised November 6, 2018; accepted January 28, 2019. Date of publication March 5, 2019; date of current version February 3, 2020. The research reported in this paper was supported by the Higher Education Excellence Program of the Ministry of Human Capacities in the frame of Artificial intelligence research area of the Budapest University of Technology and Economics (BME FIKP-MI). The Associate Editor for this paper was Z. Li. (Corresponding author: Dávid Hajdu.)

D. Hajdu is with the Department of Applied Mechanics, Budapest University of Technology and Economics, H-1111 Budapest, Hungary (e-mail: hajdu@mm.bme.hu).

J. I. Ge is with the Department of Computing and Mathematical Sciences, California Institute of Technology, Pasadena, CA 91125 USA (e-mail: gejin@umich.edu).

T. Insperger is with the Department of Applied Mechanics, Budapest University of Technology and Economics, H-1111 Budapest, Hungary, and also with the MTA-BME Lendület Human Balancing Research Group, H-1111 Budapest, Hungary (e-mail: insperger@mm.bme.hu).

G. Orosz is with the Department of Mechanical Engineering, University of Michigan, Ann Arbor, MI 48109 USA, and also with the Department of Civil and Environmental Engineering, University of Michigan, Ann Arbor, MI 48109 USA (e-mail: orosz@umich.edu).

Digital Object Identifier 10.1109/TITS.2019.2897149

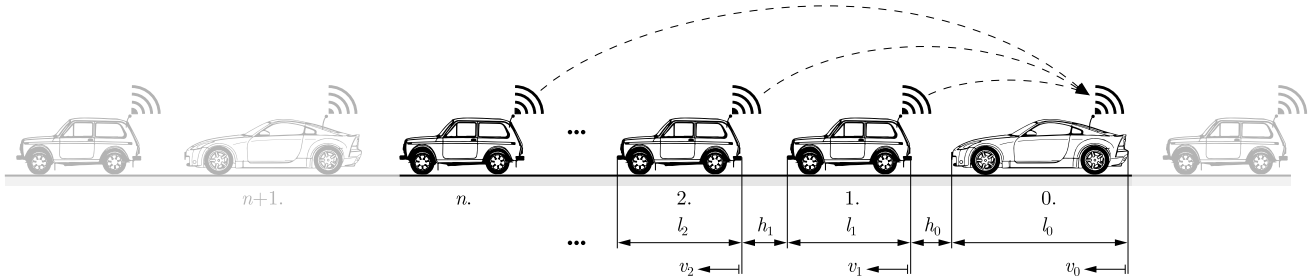


Fig. 1. A connected vehicle network arising from the V2V-based controller of a connected automated vehicle.

A distributed \mathcal{H}_∞ -controller was investigated in [24] and [25], and a similar approach with a heterogeneous vehicular platoon was studied in [26]. Some other methods were also used in [27]–[32] in order to discuss the effects of unmodeled dynamics, stochastic communication delay, measurement noise, and external disturbances.

However, the \mathcal{H}_∞ approach typically gives conservative results as pointed out in [26]. Consequently, this approach may be feasible for scenarios of limited uncertainty where all vehicles are automated and the connectivity topology is set by the designer. On the other hand, such conservativeness cannot be tolerated when a connected automated vehicle needs to respond to multiple human drivers using ad-hoc communication. There is a need for a systematic method to guarantee robust string stability against human drivers ahead with uncertain reaction time delay and feedback gains. In particular, uncertainties in the time delay must be taken into account without using conservative approximations. Moreover, the control design should allow flexible connectivity topology and scale well as the number of vehicles connected by V2X communication increases. Therefore, in this paper, we adopt structured singular value analysis [33], [34], in order to provide tight bounds for connected cruise controllers to be robustly head-to-tail string stable, despite uncertainties in human car-following behavior. We demonstrate through experimental results how this robust string stability may improve the performance of a connected automated vehicle among human-driven vehicles.

The paper is structured as follows. Sec. II introduces connected vehicle networks including the car-following models of human drivers and the structure of the controller for connected automated vehicles. Sec. III gives the detailed derivation of the uncertain model, introduces the structured singular values, and presents the results for a simple vehicle configuration. Sec. IV extends the results for large connected vehicles networks, and uses a four-vehicle system for demonstration purposes. This four-vehicle system is implemented in an experiment and the measurement results are discussed in Sec. V. Finally, in Sec. VI we reach the conclusions and provide some future research directions.

II. CONNECTED VEHICLE SYSTEMS

In this section we describe the longitudinal dynamics of a connected vehicle system. We consider a heterogeneous chain of vehicles where all vehicles are equipped with V2V

communication devices and some are capable of automated driving, as shown in Fig. 1. When an automated vehicle receives motion information broadcasted from several vehicles ahead, it may choose to use the information in its motion control (see the dashed arrows), and thus, it becomes a connected automated vehicle. Such a V2V-based controller then defines a connected vehicle network consisting of the connected automated vehicle and the preceding vehicles whose motion signals are used by the connected automated vehicle.

Inside this connected vehicle network, we denote the connected automated vehicle as vehicle 0, and the preceding vehicles as vehicles $1, \dots, n$. Note that we assume a connected automated vehicle does not “look beyond” another connected automated vehicle. For example, in Fig. 1, if vehicle 2 was also a connected automated vehicle, vehicle 0 would not include the V2V signals from vehicles farther ahead than vehicle 2 in its controller. This assumption greatly simplifies the topology of connected vehicle networks and eliminates intersections of links that are typically detrimental for the performance of the system [18], [35].

Time delays naturally arise in connected vehicle systems due to powertrain dynamics, reaction time delays of human drivers, communication delays or packet losses. The different sources of delays and effects on stability have been widely studied in the literature and have also been verified experimentally [10], [16], [25], [36]–[39]. Stability and control of platooning in the presence of time-varying delays was also investigated in [38] and [29], and predictor based designs were introduced in [40] and [41] in order to overcome the destabilizing effects of delays.

The longitudinal dynamics of vehicle i can be described by

$$\begin{aligned} \dot{h}_i(t) &= v_{i+1}(t) - v_i(t), \\ \dot{v}_i(t) &= u_i(t - \zeta_i), \end{aligned} \quad (1)$$

for $i = 0, \dots, n$, where h_i , v_i and u_i are the headway, speed and acceleration command of vehicle i , and ζ_i denotes the actuator delay. Since vehicles $1, \dots, n$ only use motion information from their immediate predecessor, their acceleration command can be described by

$$\begin{aligned} u_i(t) &= \alpha_i(V_i(h_i(t - \hat{\tau}_i)) - v_i(t - \hat{\tau}_i)) \\ &\quad + \beta_i(v_{i+1}(t - \hat{\tau}_i) - v_i(t - \hat{\tau}_i)), \end{aligned} \quad (2)$$

where $\hat{\tau}_i$ is the reaction time delay of a human driver or the sensor delay of an automated car, while α_i and β_i are the control gains. Furthermore, $V_i(h_i)$ is the range policy function

that describes the desired velocity based on headway. Here we consider

$$V_i(h_i) = \begin{cases} 0 & \text{if } h_i \leq h_{st,i}, \\ \kappa_i(h_i - h_{st,i}) & \text{if } h_{st,i} < h_i < h_{go,i}, \\ v_{\max} & \text{if } h_i \geq h_{go,i}, \end{cases} \quad (3)$$

where $\kappa_i = v_{\max}/(h_{go,i} - h_{st,i})$. That is, the desired velocity is zero for small headways ($h_i \leq h_{st,i}$) and equal to the speed limit v_{\max} for large headways ($h_i \geq h_{go,i}$). Between these, the desired velocity increases with the headway linearly, with gradient κ_i . Note that when $h_{st,i} = 0$ [m], $1/\kappa_i$ is often referred to as the time headway. Many other range policies may be chosen, but the qualitative dynamics remain similar if the above characteristics are kept.

Unlike many cooperative adaptive cruise control algorithms, the preceding vehicles $1, \dots, n$ in the connected network shown in Fig. 1 are not required to cooperate with the connected automated vehicle. That is, aside from broadcasting their motion information through V2V communication, no automation of these vehicles is required. Consequently, the feedback gains, the range policy and time delay in (2) cannot be tuned for the connected automated vehicle design. However, the connected automated vehicle 0 may fully exploit V2V signals from vehicles $1, \dots, n$ with no constraint on the connectivity topology.

Here we consider the longitudinal controller for the connected automated vehicle in the form of

$$u_0(t) = a_{1,0}(V_0(h_0(t - \hat{\sigma}_{1,0})) - v_0(t - \hat{\sigma}_{1,0})) + \sum_{j=1}^n b_{j,0}(v_j(t - \hat{\sigma}_{j,0}) - v_0(t - \hat{\sigma}_{j,0})), \quad (4)$$

where the control gains $a_{j,0}$ and $b_{j,0}$ and communication delay $\hat{\sigma}_{j,0}$ correspond to the links between vehicle j and the connected automated vehicle 0. Note that the delay $\hat{\sigma}_{j,0}$ arises from communication intermittency and possible packet losses. Here the range policy function $V_0(h_0)$ is defined as in (3) with gradient κ_0 for $h_{st,0} \leq h_0 \leq h_{go,0}$ that can be tuned by the designer together with the feedback gains $a_{j,0}$ and $b_{j,0}$.

Note that when $n = 1$, the connected automated vehicle only uses motion information from its immediate predecessor, and (4) gracefully degrades to the same control structure as human-driven vehicles [42] or automated vehicles without connectivity [4].

We consider the stability of the connected vehicle system (1,2,4) around the uniform traffic flow, where vehicles travel with the same speed $v_i(t) = v^*$ and their corresponding headways are $h_i(t) = h_i^*$ such that $V_i(h_i^*) = v^*$ for $i = 0, \dots, n$. We define the perturbations about the equilibrium (h_i^*, v^*) as

$$\tilde{h}_i(t) = h_i(t) - h_i^*, \quad \tilde{v}_i(t) = v_i(t) - v^*. \quad (5)$$

Since we are interested in how the speed perturbations \tilde{v}_i propagate through the connected vehicle system, especially how a connected automated vehicle attenuates such perturbations, we

linearize (1,2,4) around the equilibrium (h_i^*, v^*) and obtain

$$\begin{aligned} \dot{\tilde{h}}_0(t) &= \tilde{v}_1(t) - \tilde{v}_0(t), \\ \dot{\tilde{v}}_0(t) &= a_{1,0}(\kappa_0 \tilde{h}_0(t - \sigma_{1,0}) - \tilde{v}_0(t - \sigma_{1,0})) \\ &\quad + \sum_{j=1}^n b_{j,0}(\tilde{v}_j(t - \sigma_{j,0}) - \tilde{v}_0(t - \sigma_{j,0})), \\ \dot{\tilde{h}}_i(t) &= \tilde{v}_{i+1}(t) - \tilde{v}_i(t), \\ \dot{\tilde{v}}_i(t) &= \alpha_i(\kappa_i \tilde{h}_i(t - \tau_i) - \tilde{v}_i(t - \tau_i)) \\ &\quad + \beta_i(\tilde{v}_{i+1}(t - \tau_i) - \tilde{v}_i(t - \tau_i)), \quad i = 1, \dots, n, \end{aligned} \quad (6)$$

where the aggregated delays are $\sigma_{1,0} = \zeta_0 + \hat{\sigma}_{1,0}$ and $\tau_i = \zeta_i + \hat{\tau}_i$.

We assume that the connected vehicle system (6) is plant stable, that is, when the input perturbation $\tilde{v}_{n+1}(t) \equiv 0$, the perturbations \tilde{h}_i, \tilde{v}_i of the preceding vehicles and \tilde{h}_0, \tilde{v}_0 of the connected automated vehicle tend to zero regardless of the initial conditions. Then, we focus on how the connected automated vehicle responds to speed fluctuations propagating through the system. When the speed perturbation \tilde{v}_0 of the connected automated vehicle has smaller amplitude than the input \tilde{v}_n , we call the connected automated vehicle design head-to-tail string stable. Note, that while plant stability of vehicles can be guaranteed by their own parameters, head-to-tail string stability relies on the entire connected topology, and therefore it is a more severe requirement.

The notion of string stability between two consecutive vehicles was previously used to explain the amplification of speed perturbations along a chain of vehicles without connectivity [43]. However, by considering head-to-tail string stability we allow speed perturbations to be amplified among the uncontrollable vehicles $1, \dots, n$, and we focus on how the connected automated vehicle attenuates the perturbations. Being head-to-tail string stable not only enables a connected automated vehicle to enjoy better active safety, energy efficiency, and passenger comfort, it can also help to attenuate traffic waves [18].

We assume zero initial conditions for (6) and obtain

$$\begin{aligned} \tilde{V}_0(s) &= \sum_{i=1}^n T_{i,0}(s) \tilde{V}_i(s), \\ \tilde{V}_i(s) &= T_{i+1,i}(s) \tilde{V}_{i+1}(s), \end{aligned} \quad (7)$$

where $\tilde{V}_0(s)$ and $\tilde{V}_i(s)$ denote the Laplace transform of $\tilde{v}_0(t)$ and $\tilde{v}_i(t)$ for $i = 1, \dots, n$, and the link transfer functions are

$$\begin{aligned} T_{1,0}(s) &= \frac{(a_{1,0}\kappa_0 + b_{1,0}s)e^{-s\sigma_{1,0}}}{s^2 + a_{1,0}(\kappa_0 + s)e^{-s\sigma_{1,0}} + \sum_{l=1}^n b_{l,0}s e^{-s\sigma_{l,0}}}, \\ T_{i,0}(s) &= \frac{b_{i,0}s e^{-s\sigma_{i,0}}}{s^2 + a_{1,0}(\kappa_0 + s)e^{-s\sigma_{1,0}} + \sum_{l=1}^n b_{l,0}s e^{-s\sigma_{l,0}}}, \\ T_{i+1,i}(s) &= \frac{(\alpha_i \kappa_i + \beta_i s)e^{-s\tau_i}}{s^2 + (\alpha_i \kappa_i + (\alpha_i + \beta_i)s)e^{-s\tau_i}}. \end{aligned} \quad (8)$$

Thus, the head-to-tail transfer function of the connected vehicle system is

$$G_{n,0}(s) = \frac{\tilde{V}_0(s)}{\tilde{V}_n(s)} = \det(\mathbf{T}(s)), \quad (9)$$

where the transfer function matrix is

$$\mathbf{T}(s) = \begin{bmatrix} T_{1,0}(s) & -1 & 0 & \cdots & 0 \\ T_{2,0}(s) & T_{2,1}(s) & -1 & \cdots & 0 \\ \vdots & \vdots & \vdots & \ddots & \vdots \\ T_{n-1,0}(s) & T_{n-1,1}(s) & T_{n-1,2}(s) & \cdots & -1 \\ T_{n,0}(s) & T_{n,1}(s) & T_{n,2}(s) & \cdots & T_{n,n-1}(s) \end{bmatrix}, \quad (10)$$

see [18] for the proof. Note that the minors of (10) can be used to track the propagation of perturbations between any two vehicles in the system, that is, the transfer function between vehicle i and a preceding vehicle j is

$$G_{j,i}(s) = \frac{\tilde{V}_i(s)}{\tilde{V}_j(s)} = \det(\mathbf{T}_{j,i}(s)), \quad (11)$$

where $j > i$ and

$$\mathbf{T}_{j,i}(s) = \begin{bmatrix} T_{i+1,i}(s) & -1 & \cdots & 0 \\ \vdots & \vdots & \ddots & \vdots \\ T_{j-1,i}(s) & T_{j-1,i+1}(s) & \cdots & -1 \\ T_{j,i}(s) & T_{j,i+1}(s) & \cdots & T_{j,j-1}(s) \end{bmatrix}. \quad (12)$$

The criterion for head-to-tail string stability at the linear level is guaranteed if the perturbations are attenuated for any frequency, that is,

$$|\det(\mathbf{T}(i\omega))| < 1, \quad \forall \omega > 0, \quad (13)$$

where we substituted $s = i\omega$. In order to facilitate robustness analysis we rewrite (13) as

$$1 - \det(\mathbf{T}(i\omega))\delta^c \neq 0, \quad \forall \omega > 0, \quad (14)$$

where δ^c is an arbitrary complex number inside the unit circle in the complex plane, that is, $\delta^c \in \mathbb{C}$ and $|\delta^c| < 1$. Since (13, 14) only require speed fluctuations to be attenuated between the head vehicle and the automated vehicle, the human-driven vehicles in between can be string unstable. While the human drivers may amplify speed fluctuations, we assume they behave rationally, that is, they are plant stable.

To illustrate the head-to-tail string stability, here we consider a connected automated vehicle using motion information from three vehicles ahead, as shown in Fig. 2(a). The transfer function matrix for this connected vehicle system is

$$\mathbf{T}(s) = \begin{bmatrix} T_{1,0}(s) & -1 & 0 \\ T_{2,0}(s) & T_{2,1}(s) & -1 \\ T_{3,0}(s) & 0 & T_{3,2}(s) \end{bmatrix}, \quad (15)$$

where the elements $T_{1,0}(s)$, $T_{2,0}(s)$, $T_{3,0}(s)$, $T_{2,1}(s)$ and $T_{3,2}(s)$ are given by (8), while (10) results in the head-to-tail transfer function

$$G_{3,0}(s) = \det(\mathbf{T}(s)) = T_{3,0}(s) + T_{3,2}(s)T_{2,0}(s) + T_{3,2}(s)T_{2,1}(s)T_{1,0}(s). \quad (16)$$

The flow of information is illustrated on a schematic block diagram in Fig. 2(b).

We consider the case when the preceding vehicles $i = 1, 2$ have the parameters $\alpha_i = 0.2$ [1/s], $\beta_i = 0.4$ [1/s],

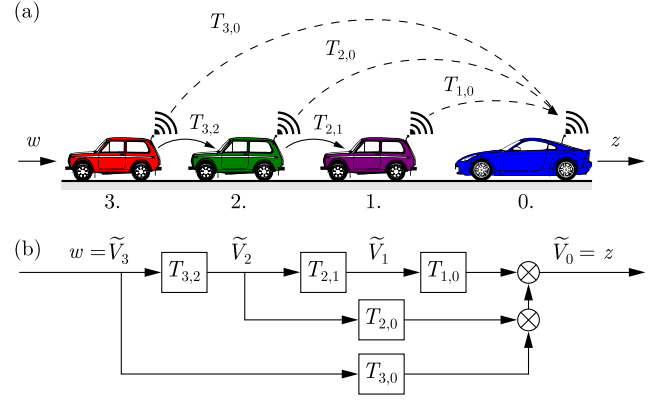


Fig. 2. A four-vehicle configuration: (a) Connected vehicle network with the information flow indicated by the dashed arrows. (b) The corresponding block diagram showing the propagation of speed perturbations $\tilde{V}_i(s)$, for $i = 3, 2, 1, 0$.

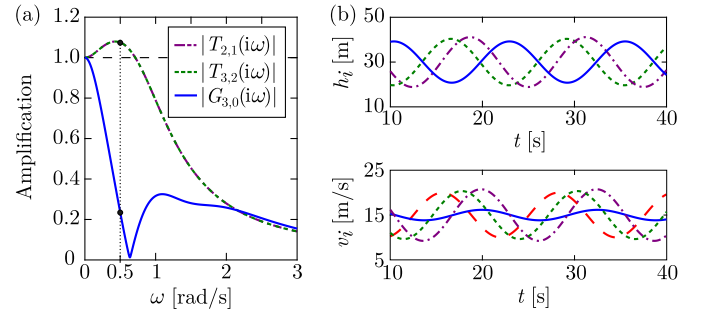
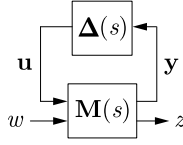


Fig. 3. (a) Example transfer functions $|T_{3,2}(i\omega)| = |T_{2,1}(i\omega)|$ and $|G_{3,0}(i\omega)|$ and (b) corresponding simulations with $v^* = 15$ [m/s], $v_3^{\text{amp}} = 5$ [m/s], and $\omega = 0.5$ [rad/s].

$\kappa_i = 0.6$ [1/s], $\tau_i = 0.9$ [s], and we set the design parameters to $a_{1,0} = 0.4$ [1/s], $b_{1,0} = 0.2$ [1/s], $b_{2,0} = 0.3$ [1/s], $b_{3,0} = 0.3$ [1/s], $\kappa_0 = 0.6$ [1/s] while having the delays $\sigma_{1,0} = \sigma_{2,0} = \sigma_{3,0} = \sigma = 0.6$ [s] for the connected automated vehicle. Human driver parameters are experimentally identified by [37], which results string unstable link transfer functions $T_{2,1}(i\omega)$ and $T_{3,2}(i\omega)$.

In Fig. 3(a) we plot the head-to-tail transfer function $|G_{3,0}(i\omega)|$ of the connected automated vehicle (solid blue curve) and the link transfer function $|T_{3,2}(i\omega)|$ that describes how vehicle 2 responds to the motion of vehicle 3 (dotted green curve). Here this is equal to $|T_{2,1}(i\omega)|$ (point-dotted purple curve) as vehicles 2 and 1 have the same parameters. While the magnitude of the head-to-tail transfer function stays below 1, the link transfer functions of vehicles 2 and 1 reach beyond 1 for low frequencies. This indicates that speed perturbations at low frequency are amplified by vehicles 2 and 1 but eventually are suppressed by the connected automated vehicle 0. This observation is supported by a simulation shown in Fig. 3(b), where the speed input $v_3(t) = v^* + v_3^{\text{amp}} \sin(\omega t)$ with $v^* = 15$ [m/s], $v_3^{\text{amp}} = 5$ [m/s], $\omega = 0.5$ [rad/s] is plotted as a dashed red curve. The time profiles for vehicles 2 and 1 are plotted by dotted green and point-dotted purple curves, respectively. The color code corresponds to the vehicle colors in Fig. 2(a).

Fig. 4. \mathbf{M} - Δ uncertain interconnection structure.

Note that the results shown in Fig. 3 strongly depend on the parameters of the preceding vehicles. The same control parameters used in Fig. 3 may behave poorly with a different set of parameters κ_i , α_i , β_i and τ_i . In the forthcoming sections, we will assume additive perturbation in these parameters denoted by $\tilde{\kappa}_i$, $\tilde{\alpha}_i$, $\tilde{\beta}_i$ and $\tilde{\tau}_i$, and apply robust control design to ensure good performance under these parameter changes.

III. ROBUST STRING STABILITY

Since a connected automated vehicle may not know the dynamics of the preceding vehicles $1, \dots, n$ accurately, the V2V-based controller should be robust against their parameter uncertainties aside from the model uncertainties of the connected automated vehicle itself. Based on the theory of robust control, we represent the system uncertainty in the \mathbf{M} - Δ uncertain interconnection structure, as shown in Fig. 4.

Here, $\mathbf{M}(s)$ represents the interconnection transfer function matrix (generalized plant) with scalar input w and scalar output z , while $\Delta(s)$ contains bounded perturbations with \mathbf{y} and \mathbf{u} as the uncertainty input and output. The uncertain interconnection structure can represent parametric and non-parametric uncertainties of the linearized system that are all contained in the matrix $\Delta(s)$. While in general the structure of $\Delta(s)$ might be arbitrary, in this work we restrict ourselves to scalar parametric uncertainties. That is, we limit the structure of the uncertainty matrix to

$$\Delta(s) = \text{diag}[\rho_1(s)\delta_1, \dots, \rho_l(s)\delta_l], \quad (17)$$

where $|\delta_k| < 1$ for $k = 1, \dots, l$, and l is the number of uncertain parameters. Note, that δ_k can be real ($\delta_k^r \in \mathbb{R}$) or complex ($\delta_k^c \in \mathbb{C}$), depending on the parameter it represents. For an introductory course in robust analysis and control, see [34], [44], or for similar studies, see [24]–[26].

Let us introduce the weight matrix

$$\mathbf{R}(s) = \text{diag}[\rho_1(s), \dots, \rho_l(s)], \quad (18)$$

which scales the uncertainties δ_k . In general the weights $\rho_k(s)$ depend on s (or later simply on ω). However, we will see that in case of parametric uncertainties they often become simple constants. Therefore, the linear model of the system with uncertainty is given by

$$\begin{bmatrix} \mathbf{y} \\ z \end{bmatrix} = \mathbf{M}(s) \begin{bmatrix} \mathbf{u} \\ w \end{bmatrix}, \quad (19)$$

$$\mathbf{u} = \Delta(s)\mathbf{y}, \quad (20)$$

with the interconnection transfer function matrix being partitioned as

$$\mathbf{M}(s) = \begin{bmatrix} \mathbf{M}_{1,1}(s) & \mathbf{M}_{1,2}(s) \\ \mathbf{M}_{2,1}(s) & M_{2,2}(s) \end{bmatrix}. \quad (21)$$

Here $M_{2,2}(s)$ is the nominal transfer function. If $\Delta(s)$ is zero, then the uncertainty drops out of the equation and only the nominal system remains.

Let $w = \tilde{V}_n(s)$ and $z = \tilde{V}_0(s)$ denote the velocity perturbations of the vehicles at the head and the tail, respectively. This yields that the transfer function between z and w equals to the head-to-tail transfer function including uncertainties. This transfer function can be expressed using upper linear fractional transformation as

$$\begin{aligned} \mathcal{F}_u(\mathbf{M}(s), \Delta(s)) \\ := M_{2,2}(s) + \mathbf{M}_{2,1}(s)\Delta(s)(\mathbf{I} - \mathbf{M}_{1,1}(s)\Delta(s))^{-1}\mathbf{M}_{1,2}(s) \end{aligned} \quad (22)$$

under the condition that

$$\det(\mathbf{I} - \mathbf{M}_{1,1}(s)\Delta(s)) \neq 0. \quad (23)$$

Observe, that if there is no uncertainty present in the system ($\Delta(s) = \mathbf{0}$), then upper linear fractional transformation gives that $M_{2,2}(s) = G_{n,0}(s)$. We also note that (23) is related to the plant stability boundaries under parametric uncertainty. Since plant stability can be guaranteed by most human drivers and automated vehicle designs, we assume that the connected automated vehicle design remains plant stable for the investigated model uncertainties.

Recall the string stability criterion (14). Similarly, the perturbed head-to-tail transfer function (22) needs to satisfy

$$1 - \mathcal{F}_u(\mathbf{M}(i\omega), \Delta(i\omega))\delta^c \neq 0, \quad \forall \omega > 0 \quad (24)$$

for any complex number $|\delta^c| < 1$. Using the Schur formula (see [45]), we rewrite (23) and (24) for $s = i\omega$ as

$$\det\left(\begin{bmatrix} \mathbf{I} & \mathbf{0} \\ \mathbf{0} & 1 \end{bmatrix} - \begin{bmatrix} \mathbf{M}_{1,1}(i\omega) & \mathbf{M}_{1,2}(i\omega) \\ \mathbf{M}_{2,1}(i\omega) & M_{2,2}(i\omega) \end{bmatrix} \begin{bmatrix} \Delta(i\omega) & \mathbf{0} \\ \mathbf{0} & \delta^c \end{bmatrix}\right) \neq 0. \quad (25)$$

Using the weight matrix $\mathbf{R}(i\omega)$, (25) can be rewritten in the compact form

$$\det(\mathbf{I} - \hat{\mathbf{M}}(i\omega)\hat{\Delta}) \neq 0, \quad (26)$$

where

$$\hat{\mathbf{M}}(i\omega) = \begin{bmatrix} \mathbf{M}_{1,1}(i\omega)\mathbf{R}(i\omega) & \mathbf{M}_{1,2}(i\omega) \\ \mathbf{M}_{2,1}(i\omega)\mathbf{R}(i\omega) & M_{2,2}(i\omega) \end{bmatrix}, \quad (27)$$

$$\hat{\Delta} = \text{diag}[\delta_1, \dots, \delta_l, \delta^c]. \quad (28)$$

Note, that while δ_k , $k = 1, \dots, l$ represent parametric uncertainty, δ^c is required to fulfill robust string stability (robust performance).

A. Robust String Stable Example

In order to quantify the robustness of the system, we use the structured singular value analysis introduced in [33]. We define the μ -value of $\hat{\mathbf{M}}(i\omega)$ as the inverse of the smallest $\bar{\sigma}(\hat{\Delta})$ when (26) fails at frequency ω , i.e.,

$$\mu(\omega) = \left(\min_{\hat{\Delta}} \{\bar{\sigma}(\hat{\Delta}) : \det(\mathbf{I} - \hat{\mathbf{M}}(i\omega)\hat{\Delta}) = 0\} \right)^{-1}, \quad (29)$$

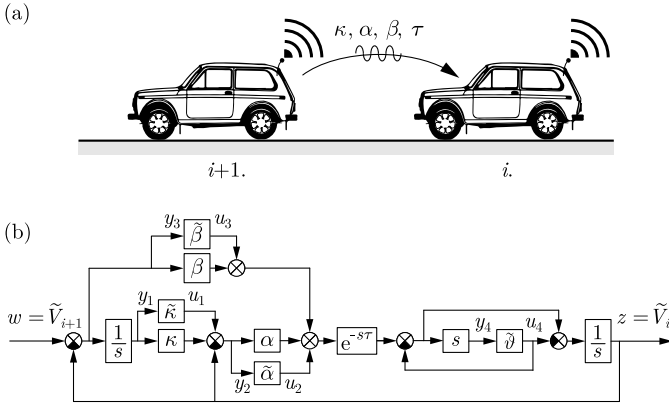


Fig. 5. (a) Predecessor-follower model; (b) Block diagram of the uncertain transfer function.

where $\bar{\sigma}(\hat{\Delta})$ denotes the largest singular value of $\hat{\Delta}$. As $\mu(\omega)$ increases, a smaller perturbation value in $\hat{\Delta}$ may lead to a singular $(\mathbf{I} - \hat{\mathbf{M}}(i\omega)\hat{\Delta})$ and results in string instability. When singularity holds for arbitrarily small perturbations, then $\mu(\omega) \rightarrow \infty$ and robustness cannot be guaranteed, however, if $\det(\mathbf{I} - \hat{\mathbf{M}}(i\omega)\hat{\Delta}) \neq 0$ for any perturbation $\hat{\Delta}$, then $\mu(\omega) = 0$. Therefore, the condition for robust string stability against bounded parameter variation is

$$\mu(\omega) < 1, \quad \forall \omega > 0, \quad (30)$$

otherwise there exists a perturbation matrix $\hat{\Delta}$, $\bar{\sigma}(\hat{\Delta}) < 1$ such that $\det(\mathbf{I} - \hat{\mathbf{M}}(i\omega)\hat{\Delta}) = 0$.

The definition of μ according to (29) does not yield directly any tractable way to compute it, since the optimization problem is not convex in general, therefore multiple local extrema might exist [46]. Instead, we are interested in computing upper ($\mu(\omega) \leq \bar{\mu}(\omega)$) and/or lower bounds ($\underline{\mu}(\omega) \leq \mu(\omega)$), for which several alternative formulations have been developed, see [33], [46]–[48]. In this paper, we use the `mussv` function in MATLAB μ -Analysis and Synthesis Toolbox [49], which implements these algorithms, and we only focus on the results, not on the numerical issues.

As an illustration of the robust string stability, we consider vehicle i that only uses information from one vehicle ahead; see Fig. 5(a). In this case the input of the nominal system is $\tilde{v}_{i+1}(t)$ while the output is $\tilde{v}_i(t)$. The nominal link transfer function is given by

$$T_{i+1,i}(s) = \frac{(\alpha\kappa + \beta s)e^{-s\tau}}{s^2 + (\alpha\kappa + (\alpha + \beta)s)e^{-s\tau}}, \quad (31)$$

where, for the sake of brevity, we dropped the subscripts of the parameters κ , α , β , and τ ; cf. (8).

While the additive uncertainties $\tilde{\alpha}$, $\tilde{\beta}$, and $\tilde{\kappa}$ result in additive uncertainty terms, an additive delay uncertainty $\tilde{\tau}$ will result in a multiplicative exponential term $e^{-s\tilde{\tau}}$ in (31), that is,

$$\begin{aligned} T_{i+1,i}(s) + \tilde{T}_{i+1,i}(s) &= \frac{((\kappa + \tilde{\kappa})(\alpha + \tilde{\alpha}) + (\beta + \tilde{\beta})s)e^{-s(\tau + \tilde{\tau})}}{s^2 + ((\kappa + \tilde{\kappa})(\alpha + \tilde{\alpha}) + (\alpha + \tilde{\alpha} + \beta + \tilde{\beta})s)e^{-s(\tau + \tilde{\tau})}}, \end{aligned} \quad (32)$$

where $\tilde{T}_{i+1,i}(s)$ represents the uncertainty while the nominal part $T_{i+1,i}(s)$ is given by (31). In order to clearly separate the model of the single vehicle from the connected vehicle structure, we introduce the notation $\mathbf{m}\text{-}\delta$ and use lower case letters for the single car scenario. In case of multiple vehicles, $\mathbf{M}(s)$ and $\mathbf{\Delta}(s)$ can be built up systematically from the link transfer functions $T_{j,i}(s)$, matrices $\mathbf{m}(s)$ and uncertainties $\delta(s)$ of individual vehicles (see Sec. IV).

To formulate the uncertainties in a way that can be represented by the $\mathbf{m}\text{-}\delta$ interconnection structure (19-20), and make the robust analysis feasible, we use the Rekasius substitution

$$e^{-s\tilde{\tau}} = \frac{1 - s\tilde{\vartheta}(s)}{1 + s\tilde{\vartheta}(s)}, \quad (33)$$

where we restrict ourselves to $s = i\omega$ and therefore we have

$$\tilde{\vartheta}(i\omega) = \frac{1}{\omega} \tan \frac{\omega\tilde{\tau}}{2}, \quad (34)$$

see [50]. This substitution is exact in the region $0 \leq \omega < \pi/\tilde{\tau}$, since it covers the same domain on the complex plane as $e^{-i\omega\tilde{\tau}}$.

By taking into account the uncertain parameters (and the Rekasius substitution), the block diagram in Fig. 5(b) can be drawn. This illustrates how uncertainties affect the system and allows us to construct the $\mathbf{m}\text{-}\delta$ uncertain interconnection structure by solving a number of algebraic equations. In particular, we define the interconnection transfer function matrix $\mathbf{m}(s)$ for a single vehicle by (35-36), as shown at the bottom of this page, where the matrix of uncertainties read

$$\delta(s) = \text{diag}[\tilde{\kappa}, \tilde{\alpha}, \tilde{\beta}, \tilde{\vartheta}(s)], \quad (37)$$

cf. (17). Therefore using (22), the perturbed link transfer function can be written as

$$\begin{aligned} \mathcal{F}_u(\mathbf{m}(s), \delta(s)) &= T_{i+1,i}(s) + \tilde{T}_{i+1,i}(s) \\ &= \underbrace{\underline{m}_{2,2}(s)}_{T_{i+1,i}(s)} + \underbrace{\underline{m}_{2,1}(s)\delta(s)(\mathbf{I} - \underline{m}_{1,1}(s)\delta(s))^{-1}\underline{m}_{1,2}(s)}_{\tilde{T}_{i+1,i}(s)} \end{aligned}$$

$$\mathbf{m}(s) = \frac{1}{D(s)} \begin{bmatrix} -ae^{-s\tau} & -e^{-s\tau} & -e^{-s\tau} & -2 & s + ae^{-s\tau} \\ s^2 + \beta se^{-s\tau} & -(\kappa + s)e^{-s\tau} & -(\kappa + s)e^{-s\tau} & 2(\kappa + s) & \kappa s - \beta se^{-s\tau} \\ -ase^{-s\tau} & -se^{-s\tau} & -se^{-s\tau} & 2s & s^2 + ase^{-s\tau} \\ as^3e^{-s\tau} & s^3e^{-s\tau} & s^3e^{-s\tau} & -s^3 + s(\kappa\alpha + s(\alpha + \beta))e^{-s\tau} & (\kappa as^2 + \beta s^3)e^{-s\tau} \\ ase^{-s\tau} & se^{-s\tau} & se^{-s\tau} & -2s & (\kappa\alpha + \beta s)e^{-s\tau} \end{bmatrix}, \quad (35)$$

$$D(s) = s^2 + (\kappa\alpha + s(\alpha + \beta))e^{-s\tau}, \quad (36)$$

TABLE I

UNCERTAINTIES IN THE PREDECESSOR-FOLLOWER VEHICLE MODEL

Parameter/ Performance	Uncertainty and representation	Weight	Type
Gradient κ	$\kappa + \tilde{\kappa} = \kappa + \rho_1 \delta_1^r$	ρ_1	$\delta_1^r \in \mathbb{R}$
Gain α	$\alpha + \tilde{\alpha} = \alpha + \rho_2 \delta_2^r$	ρ_2	$\delta_2^r \in \mathbb{R}$
Gain β	$\beta + \tilde{\beta} = \beta + \rho_3 \delta_3^r$	ρ_3	$\delta_3^r \in \mathbb{R}$
Time delay τ	$e^{-s(\tau+\tilde{\tau})} = e^{-s\tau} \frac{1-s\rho_4(s)\delta_4^r}{1+s\rho_4(s)\delta_4^r}$	$\rho_4(s)$	$\delta_4^r \in \mathbb{R}$
Robust performance	$1 - \mathcal{F}_u(\mathbf{m}(i\omega), \delta(i\omega))\delta^c \neq 0$	1	$\delta^c \in \mathbb{C}$

$$= \frac{((\kappa + \tilde{\kappa})(\alpha + \tilde{\alpha}) + (\beta + \tilde{\beta})s)e^{-s\tau} \frac{1-s\tilde{\nu}(s)}{1+s\tilde{\nu}(s)}}{s^2 + ((\kappa + \tilde{\kappa})(\alpha + \tilde{\alpha}) + (\alpha + \tilde{\alpha} + \beta + \tilde{\beta})s)e^{-s\tau} \frac{1-s\tilde{\nu}(s)}{1+s\tilde{\nu}(s)}}. \quad (38)$$

The only difference compared to (32) is the Rekasius substitution, which is still exact for $s = i\omega$. Note that there exist other ways to approximate the uncertainty in the time-delay, for instance by replacing $e^{-s\tilde{\tau}}$ with a complex term $g(s)$ directly, see [51]. However, this typically leads to a conservative solution.

In order to utilize the robust calculation and μ -analysis, we introduce the weight matrix

$$\mathbf{r}(s) = \text{diag}[\rho_1, \rho_2, \rho_3, \rho_4(s)], \quad (39)$$

where

$$\tilde{\kappa} = \rho_1 \delta_1^r, \quad \tilde{\alpha} = \rho_2 \delta_2^r, \quad \tilde{\beta} = \rho_3 \delta_3^r, \quad \tilde{\nu}(s) = \rho_4(s) \delta_4^r, \quad (40)$$

cf. (18). Thus, the rescaled matrix (28) reads

$$\hat{\delta} = \text{diag}[\delta_1^r, \delta_2^r, \delta_3^r, \delta_4^r, \delta^c], \quad (41)$$

where upper index indicates whether the uncertainty is real ($\delta_k^r \in \mathbb{R}$) or complex ($\delta_k^c \in \mathbb{C}$), and

$$\hat{\mathbf{m}}(i\omega) = \begin{bmatrix} \mathbf{m}_{1,1}(i\omega)\mathbf{r}(i\omega) & \mathbf{m}_{1,2}(i\omega) \\ \mathbf{m}_{2,1}(i\omega)\mathbf{r}(i\omega) & m_{2,2}(i\omega) \end{bmatrix}, \quad (42)$$

cf. (27) and (28). The list of the uncertain parameters and their representations are given in Table I. Then with the use of the MATLAB command `mussv` [49], the structured singular value of $\hat{\mathbf{m}}(i\omega)$ can be calculated for different values of ω .

The parameter κ may be increased/decreased depending on the driver/passenger preferences and the value of τ is influenced by the powertrain and the automated driving system (or the human driver reaction time). Thus, we assume nonzero parameter uncertainties $\tilde{\kappa}$ and $\tilde{\tau}$, set $\tilde{\alpha} = 0$, $\tilde{\beta} = 0$, and plot the robust string stable regions in the (β, α) -plane. In particular, we quantify $\tilde{\kappa}$ and $\tilde{\tau}$ using nominal values with variations. For example, 10% in κ indicates that the parameter has maximum 10% uncertainty in its nominal value ($\rho_1 = 0.1\kappa$ in (39)). For simplicity, we assume the same relative uncertainty for κ and τ . In order to speed up the calculations, the bisection algorithm developed in [52] is utilized, and only the boundary is searched.

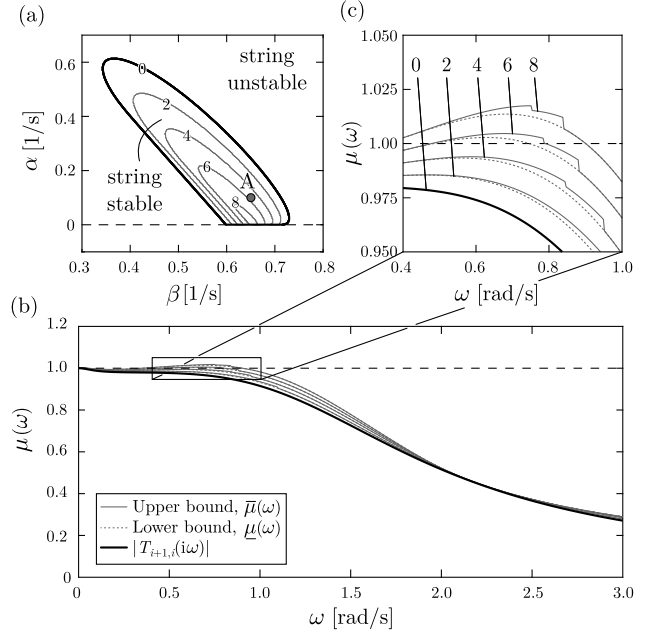


Fig. 6. (a) Robust stability charts in the (β, α) -plane for $\kappa = 0.6$ [1/s], $\tau = 0.7$ [s] with uncertainties 0, 2, 4, 6, 8%, where black curve indicates the nominal string stability boundary and gray curves indicate the robust string stability boundaries. (b) The nominal transfer function $|T_{i+1,i}(i\omega)|$ (black) and $\mu(\omega)$ curves (gray) for point A ($\alpha = 0.1$ [1/s], $\beta = 0.65$ [1/s]). (c) Zoom in of the critical region, where $\mu(\omega) > 1$.

For parameter values $\kappa = 0.6$ [1/s], $\tau = 0.7$ [s], the nominal (black) and robust (gray) string stability boundaries are shown in Fig. 6(a). In this case string stable domain exists when $\tau < 1/(2\kappa) \approx 0.833$ [s]. As the uncertainty in κ and τ increases, the robust string stable area shrinks. Note that when uncertainty goes above 8%, the robust stable domain completely disappears.

We pick the point A ($\alpha = 0.1$ [1/s], $\beta = 0.65$ [1/s]) in Fig. 6(a), and plot the corresponding $\mu(\omega)$ and nominal $|T_{i+1,i}(i\omega)|$ curves in Fig. 6(b-c). The absolute value of the link transfer function is shown by black curve, while the gray curves correspond to the $\mu(\omega)$ curves for different uncertainties. Recall that the real μ -values cannot be determined exactly, so rather upper bounds ($\bar{\mu}$ - solid gray) and lower bounds ($\underline{\mu}$ - dashed gray) are computed. Details in the critical region can be seen in Fig. 6(c), where only a slight difference between the upper and lower bounds can be observed. This results very small conservativeness, and therefore for a safer approximation we assume that $\mu(\omega) \approx \bar{\mu}(\omega)$. If $\bar{\mu}(\omega)$ remains below 1, then robustness is guaranteed for that perturbation level. Otherwise, the system can lose string stability around the frequency where $\bar{\mu}(\omega)$ is above 1. For example, the α, β combination at point A is robust against 4% uncertainty, and leads to string unstable behavior at 6%.

IV. ROBUST STRING STABLE DESIGN FOR CONNECTED AUTOMATED VEHICLES

In this section, we first introduce a systematic method to extend the robust head-to-tail string stability analysis to general connected vehicle systems. This yields a linear fractional transformation model, which can be formulated for

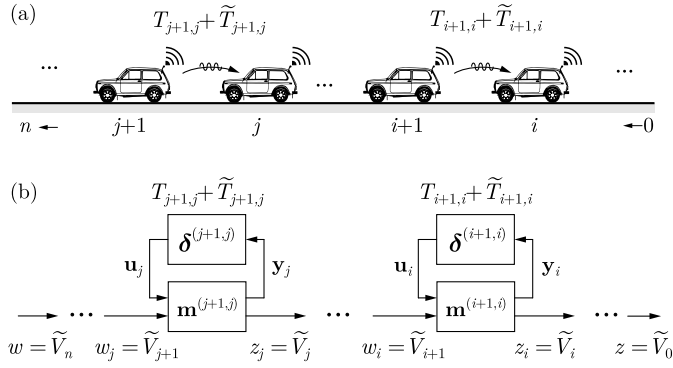


Fig. 7. (a) Chain of connected vehicles with uncertain dynamics. (b) Corresponding block diagram.

arbitrary connected vehicle networks with various topology and uncertainty. Then, we demonstrate the method in a connected automated vehicle design where motion information from three vehicles ahead is used.

A. Scaling Up the Generalized Plant Matrix

Recall that for the robustness analysis in Sec. III-A, we deduced the interconnection transfer function matrix $\mathbf{m}(s)$ graphically using the block diagram in Fig. 5(b). However, as the number of vehicles in a connected vehicle system increases, it is desirable to obtain such matrices algebraically in a systematic manner. Specifically, we treat each vehicle in the connected vehicle system as a subsystem whose uncertainty is described by an \mathbf{m} - δ structure as in Sec. III-A. Then we exploit the topology of the connected vehicle system and assemble the \mathbf{M} - Δ structure. Note that this formalism allows us to incorporate the uncertainty for an arbitrary number of human drivers, making this method scaleable for large connected vehicle systems.

Again we consider a connected automated vehicle using motion information from n human-driven vehicles ahead, as shown in Fig. 1. Consider the set \mathcal{D} of vehicles with uncertainties (not necessarily all of the vehicles in the system are uncertain), where $\mathcal{D} \subseteq \{1, \dots, n\}$. Based on (19-20), the uncertainty model for vehicle $i \in \mathcal{D}$ with respect to vehicle $i+1$ is

$$\begin{aligned} \mathbf{y}_i &= \mathbf{m}_{1,1}^{(i+1,i)}(s)\mathbf{u}_i + \mathbf{m}_{1,2}^{(i+1,i)}(s)w_i, \\ z_i &= \mathbf{m}_{2,1}^{(i+1,i)}(s)\mathbf{u}_i + m_{2,2}^{(i+1,i)}(s)w_i, \end{aligned} \quad (43)$$

where superscript $(i+1, i)$ denotes the uncertain link between vehicles $i+1$ and i , see Fig. 7. Note that $m_{2,2}^{(i+1,i)}(s) = T_{i+1,i}(s)$, as in Sec. III-A.

Now we can exploit the cascading topology of the system, as vehicles only respond to perturbations from their immediate predecessor, i.e., the input w_i of vehicle i is the output z_{i+1} of vehicle $i+1$. Therefore, we define $w = \tilde{V}_n$, $z = \tilde{V}_0$, and expand the model (43) by including uncertainties \mathbf{u}_p from all preceding vehicle $p \in \mathcal{D} \cap \{i+1, \dots, n\}$, that is,

$$\begin{aligned} \mathbf{y}_i &= \mathbf{m}_{1,1}^{(i+1,i)}(s)\mathbf{u}_i + \mathbf{m}_{1,2}^{(i+1,i)}(s)G_{n,i+1}(s)w \\ &+ \sum_{p=i+1}^n \mathbf{m}_{1,2}^{(i+1,i)}(s)\mathbf{m}_{2,1}^{(p+1,p)}(s)G_{p,i+1}(s)\mathbf{u}_p, \end{aligned} \quad (44)$$

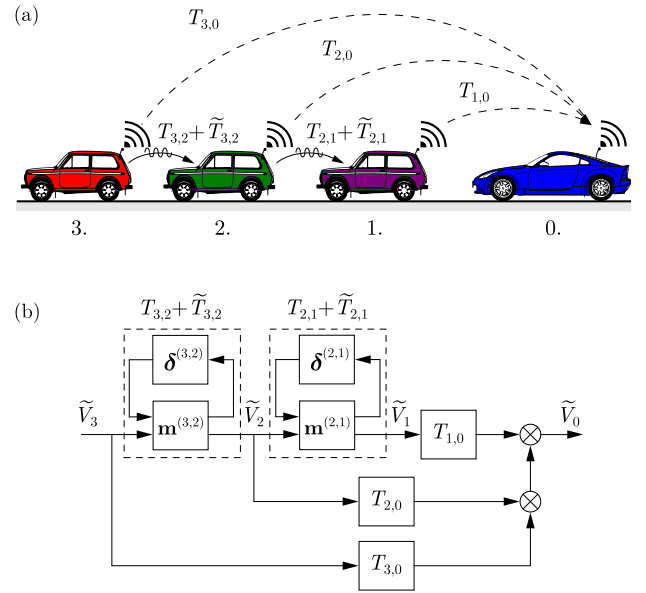


Fig. 8. Four-vehicle configuration with uncertainties: (a) Connectivity topology; (b) Block diagram.

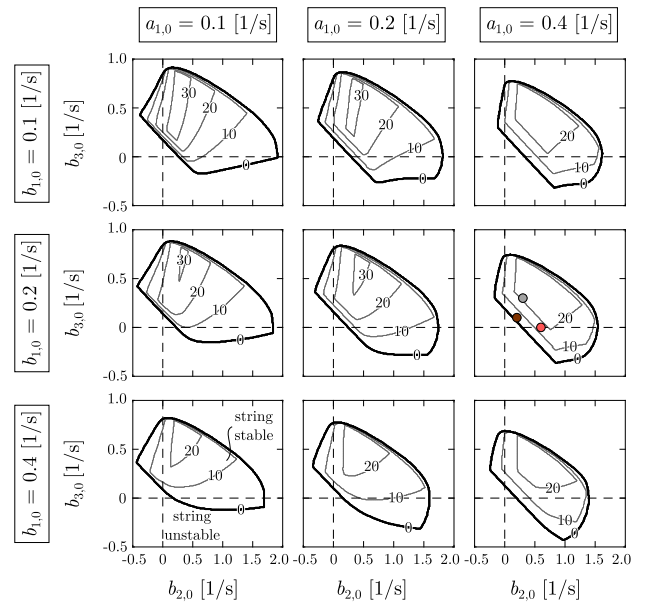


Fig. 9. Robust stability charts in the $(b_{2,0}, b_{3,0})$ -plane for different values of $a_{1,0}$ and $b_{1,0}$. The nominal human driver parameters are $\kappa_i = 0.6$ [1/s], $\alpha_i = 0.2$ [1/s], $\beta_i = 0.4$ [1/s] and $\tau_i = 0.9$ [s] for $i = 1, 2$, and the connected automated vehicle has $\kappa_0 = 0.6$ [1/s] and $\sigma = 0.6$ [s]. Robust string stable boundaries are indicated by gray curves in case of 0, 10, 20, 30% uncertainty.

where summation only includes the uncertain vehicles, $G_{j,i}(s)$ is defined in (11) and $G_{i,i}(s) = 1$.

This way, we construct the uncertain \mathbf{M} - Δ interconnection structure as

$$\begin{bmatrix} \vdots \\ \mathbf{y}_i \\ \vdots \\ z \end{bmatrix} = \underbrace{\begin{bmatrix} \vdots & \vdots \\ \cdots & [\mathbf{M}_{1,1}(s)]_{i,j} & \cdots & [\mathbf{M}_{1,2}(s)]_i \\ \vdots & \vdots \\ \cdots & [\mathbf{M}_{2,1}(s)]_j & \cdots & M_{2,2}(s) \end{bmatrix}}_{\mathbf{M}(s)} \begin{bmatrix} \vdots \\ \mathbf{u}_j \\ \vdots \\ w \end{bmatrix}, \quad (45)$$

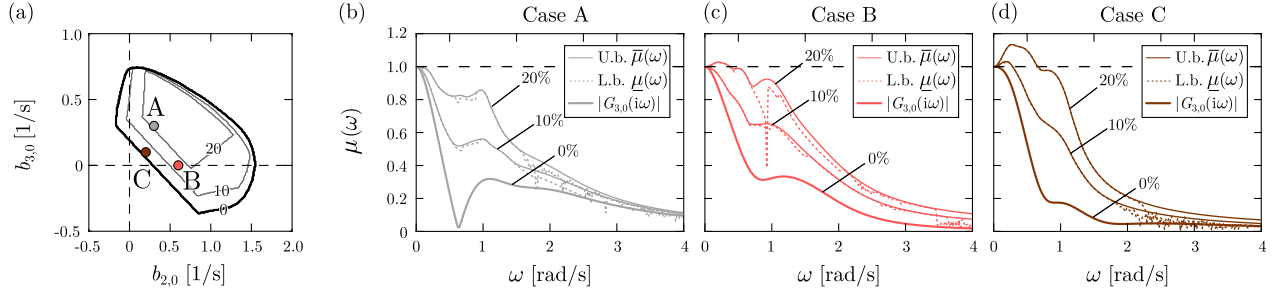


Fig. 10. (a) Robust stability charts for $a_{1,0} = 0.4$ [1/s] and $b_{1,0} = 0.2$ [1/s]. (b)-(d) $|G_{3,0}(i\omega)|$ and $\mu(\omega)$ curves for points (A,B,C) and uncertainty levels 0, 10, 20%.

where the elements in $\mathbf{M}(s)$ can be obtained systematically:

$$[\mathbf{M}_{1,1}(s)]_{i,j} = \begin{cases} \mathbf{m}_{1,2}^{(i+1,i)}(s)\mathbf{m}_{2,1}^{(j+1,j)}(s)G_{j,i+1}(s), & \text{if } j > i, \\ \mathbf{m}_{1,1}^{(i+1,i)}(s), & \text{if } j = i, \\ \mathbf{0}, & \text{if } j < i, \end{cases} \quad (46)$$

$$[\mathbf{M}_{1,2}(s)]_i = \mathbf{m}_{1,2}^{(i+1,i)}(s)G_{n,i+1}(s), \quad (47)$$

$$[\mathbf{M}_{2,1}(s)]_j = \mathbf{m}_{2,1}^{(j+1,j)}(s)G_{j,0}(s), \quad (48)$$

$$M_{2,2}(s) = G_{n,0}(s), \quad (49)$$

for $i, j \in \mathcal{D}$.

Meanwhile, the uncertainty matrix is formulated as

$$\begin{bmatrix} \vdots \\ \mathbf{u}_i \\ \vdots \end{bmatrix} = \underbrace{\begin{bmatrix} \ddots & & & & \\ & \delta^{(i+1,i)}(s) & & & \\ & & \ddots & & \\ & & & \ddots & \\ & & & & \ddots \end{bmatrix}}_{\mathbf{\Delta}(s)} \begin{bmatrix} \vdots \\ \mathbf{y}_i \\ \vdots \end{bmatrix}, \quad (50)$$

and weight matrix is constructed as

$$\mathbf{R}(s) = \text{diag} \left[\dots, \mathbf{r}^{(i+1,i)}(s), \dots \right], \quad (51)$$

where $\delta^{(i+1,i)}(s)$ and $\mathbf{r}^{(i+1,i)}(s)$ are the uncertainty matrix and weight matrix corresponding to vehicle i (cf. (37) and (39)). Finally, robustness is guaranteed if

$$\det(\mathbf{I} - \hat{\mathbf{M}}(i\omega)\hat{\mathbf{\Delta}}) \neq 0, \quad (52)$$

where

$$\hat{\mathbf{M}}(i\omega) = \begin{bmatrix} \mathbf{M}_{1,1}(i\omega)\mathbf{R}(i\omega) & \mathbf{M}_{1,2}(i\omega) \\ \mathbf{M}_{2,1}(i\omega)\mathbf{R}(i\omega) & M_{2,2}(i\omega) \end{bmatrix}, \quad (53)$$

$$\hat{\mathbf{\Delta}} = \text{diag} [\delta_1^r, \dots, \delta_l^r, \delta^c]. \quad (54)$$

B. Robust String Stability in a Four-Vehicle System

In order to demonstrate the applicability of the algorithm, we present a case study for a connected vehicle system consisting of a connected automated vehicle and three human-driven cars with uncertainty, i.e., $n = 3$ in (6). The sketch of the system is displayed in Fig. 8(a) while the block diagram with uncertainties is presented in Fig. 8(b), cf. Fig. 2(b). While the nominal transfer function matrix is given in (15), we assume each parameter in vehicles 2 and 1 has uncertainty



Fig. 11. (a) Two human-driven vehicles and one connected automated vehicle used in the experiments. The two vehicles on the left are only equipped with V2V communication devices, while the vehicle on the right is capable of automated driving as well as V2V communication. (b) The V2V communication on-board unit: ① upper-level computer, ② ethernet cable, ③ electronic control unit, ④ power cable, ⑤ V2V/GPS antennae.

and compute the robust string stable regions in the $(b_{2,0}, b_{3,0})$ -plane for different values of $a_{1,0}$ and $b_{1,0}$.

The uncertain interconnection structure is given as

$$\mathbf{M}(s) = \begin{bmatrix} \mathbf{m}_{1,1}^{(2,1)} & \mathbf{m}_{1,2}^{(2,1)} & \mathbf{m}_{2,1}^{(3,2)} & \mathbf{m}_{12}^{(2,1)}T_{3,2} \\ \mathbf{0} & \mathbf{m}_{1,1}^{(3,2)} & \mathbf{m}_{1,1}^{(3,2)} & \mathbf{m}_{1,2}^{(3,2)} \\ \mathbf{m}_{2,1}^{(2,1)}T_{1,0} & \mathbf{m}_{2,1}^{(3,2)}(T_{2,0} + T_{1,0}T_{2,1}) & \mathbf{m}_{1,1}^{(3,2)} & G_{3,0} \end{bmatrix}, \quad (55)$$

where the dependence on s is not spelled out for conciseness, while the weight matrix reads

$$\mathbf{R}(s) = \begin{bmatrix} \mathbf{r}^{(2,1)}(s) & \mathbf{0} \\ \mathbf{0} & \mathbf{r}^{(3,2)}(s) \end{bmatrix}. \quad (56)$$

The robust performance is given by (52-54), where $l = 8$ corresponds to the 4 + 4 independent parameters of vehicles 1 and 2.

The computation of μ -values are performed by the MATLAB toolbox using the `mussv` function. The results are presented in Fig. 9 and Fig. 10, where we assumed that each parameter of each vehicle is perturbed by the same percentage of their nominal value, i.e., $\alpha_i, \beta_i, \kappa_i$ and τ_i have identical relative uncertainties. The nominal human driver parameters are $\kappa_i = 0.6$ [1/s], $\alpha_i = 0.2$ [1/s], $\beta_i = 0.4$ [1/s] and

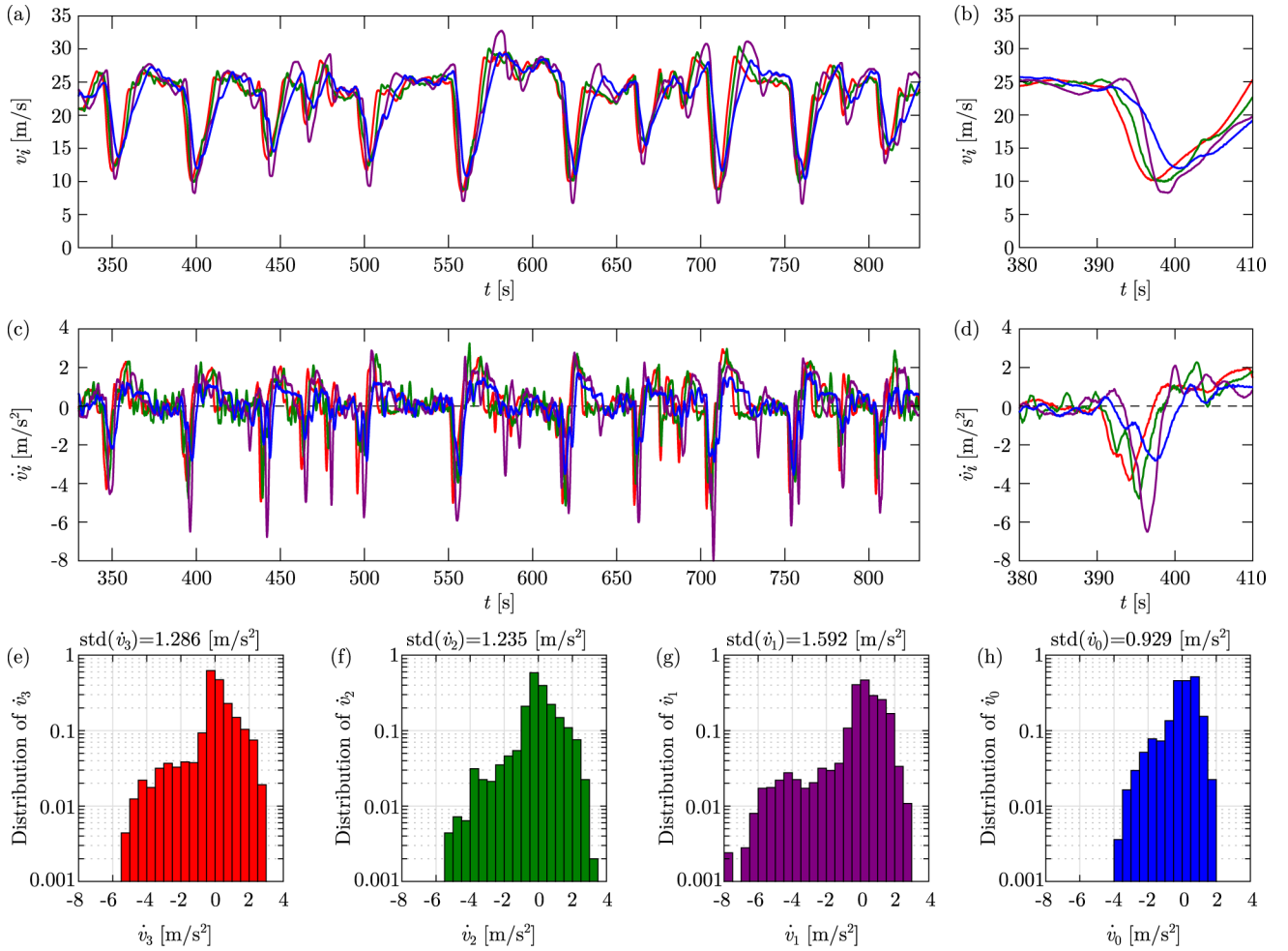


Fig. 12. Measurement at point A in Fig. 10(a): (a-b) Measured speed profiles of three human-driven vehicles and automated vehicle; (c-d) Acceleration profiles; (e-h) Normalized histograms showing the distributions of accelerations. The graphs are colored corresponding to the color of vehicles in Fig. 8(a).

$\tau_i = 0.9$ [s] (same for both vehicles for simplicity), while the fixed parameters of the connected automated vehicle are $\kappa_0 = 0.6$ [1/s] and $\sigma = 0.6$ [s]. In this configuration, human-driven vehicles are string unstable, but head-to-tail string stability can be guaranteed by appropriate selection of the gains of the connected automated vehicle. Fig 9. shows how the uncertain parameters (eight in total) affect the robust stable domain of control parameters $(a_{1,0}, b_{1,0}, b_{2,0}, b_{3,0})$. While the nominal system (black curve) provides a relatively large string stable domain, uncertainty significantly reduces it (gray curves) and having uncertainty greater than 30% eliminates the robust boundaries in most of the cases.

In order to further illustrate the effects of uncertainty, we choose three different control gain pairs in Fig. 10(a) and plot the corresponding $\mu(\omega)$ curves in Fig. 10(b-d) for different uncertainty levels. Point A (gray) is inside the 20% robustness region and corresponds to $b_{2,0} = 0.3$ [1/s], $b_{3,0} = 0.3$ [1/s], point B (light red) is inside the 10% robustness region and denotes $b_{2,0} = 0.6$ [1/s], $b_{3,0} = 0.0$ [1/s], while point C (brown) is outside the 10% robust region, but still inside the string stable domain and its parameters are $b_{2,0} = 0.2$ [1/s], $b_{3,0} = 0.1$ [1/s]. Colored thick curves indicate the value of $|G_{3,0}(i\omega)|$, while colored thin curves

indicate $\mu(\omega)$ at 10% and 20% uncertainty levels. In each case the continuous curve is the upper bound $\bar{\mu}$, while dashed curve is the lower bound $\underline{\mu}$. The color code used in panel (a) matches the colors on panels (b-d). Similarly to the example shown in Sec. III-A, the shape of μ -plots are similar to the absolute values of the transfer functions. Where the $\bar{\mu}(\omega)$ goes above 1, the system loses string stability around that frequency. If $\bar{\mu}(\omega)$ remains below 1, then robustness is guaranteed for the corresponding perturbation level.

V. EXPERIMENTAL VALIDATION OF ROBUST STRING-STABLE DESIGN

In this section we experimentally evaluate the performance of connected cruise control designs with different levels of robustness. We demonstrate that robust string stable design is able to ensure less harsh maneuvers for a connected automated vehicle operating among human-driven vehicles.

We consider the scenario shown in Fig. 8(a), where one connected automated vehicle drives behind three human-driven vehicles. The connected automated vehicle and two human-driven vehicles used in the experiments are shown in Fig. 11(a). The speed and position data of each vehicle

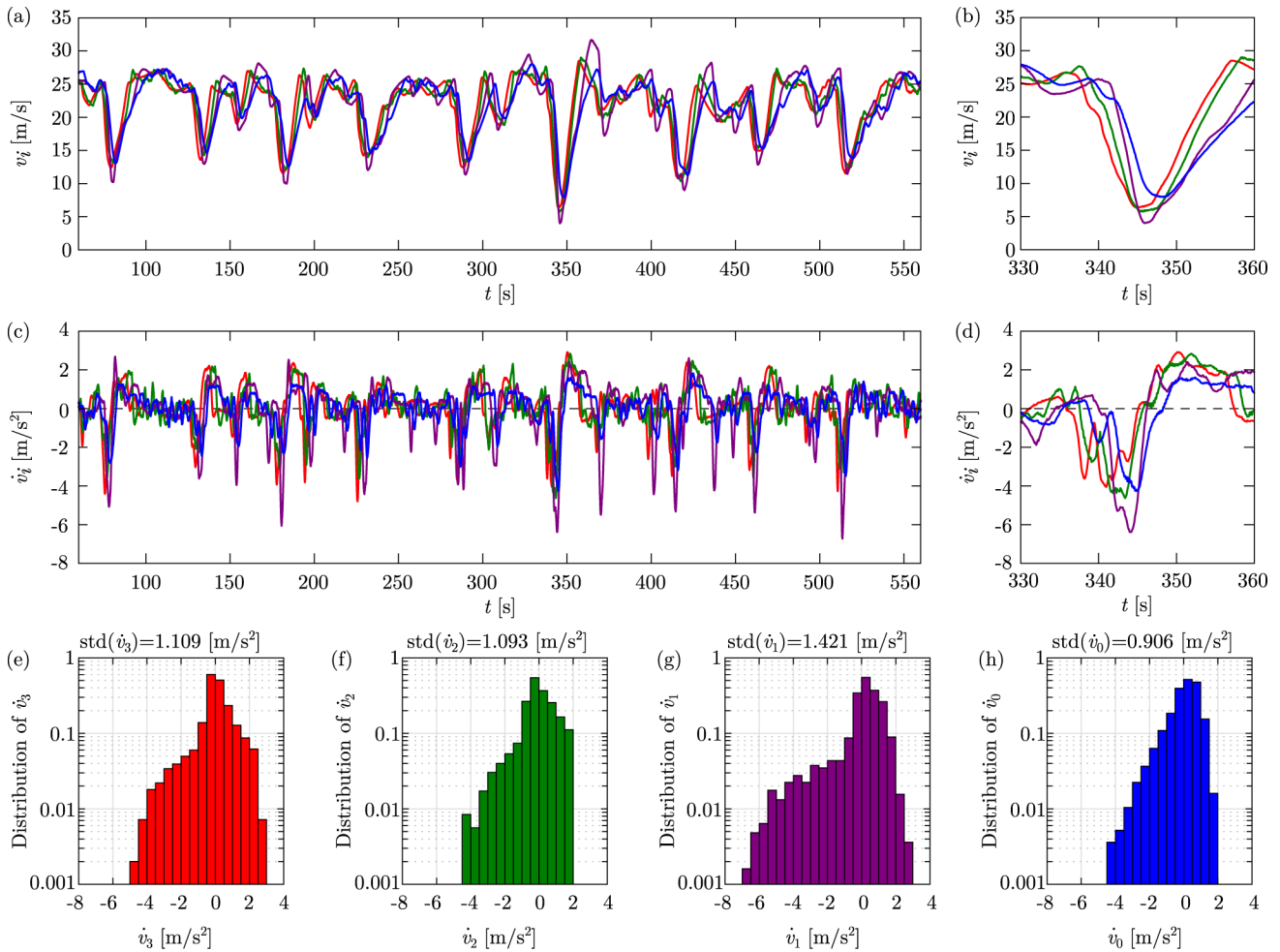


Fig. 13. Measurement at point B in Fig. 10(a): (a-b) Measured speed profiles of three human-driven vehicles and automated vehicle; (c-d) Acceleration profiles; (e-h) Normalized histograms showing the distributions of accelerations. The graphs are colored corresponding to the color of vehicles in Fig. 8(a).

are recorded and transmitted with 10 Hz update rate through dedicated short range communication (DSRC) using V2V devices shown in Fig. 11(b) [53]. We note that while all vehicles are equipped with V2V communication devices, only one vehicle (right) is automated using the connected cruise controller (4). Further details about the setup and experimental results are given in [36]. In this paper, we present two sets of experiments for demonstration purposes.

Test drives are conducted on a segment of single-lane public road where vehicles experience a series of braking events due to dense traffic. The results from the first experiment set are shown in Fig. 12, where the connected automated vehicle adopts a 20%-robust string-stable design $(a_{1,0}, b_{1,0}, b_{2,0}, b_{3,0}) = (0.4, 0.2, 0.3, 0.3)$ [1/s], i.e., case A in Fig 10(a). The results from the second experiment set are plotted in Fig. 13, where the connected automated vehicle adopts a 10%-robust string-stable design $(a_{1,0}, b_{1,0}, b_{2,0}, b_{3,0}) = (0.4, 0.2, 0.6, 0.0)$ [1/s], i.e., case B in Fig 10(a). We note that while both cases ensure head-to-tail string stability when the human car-following parameters deviate from their nominal values by up to 10%, case B loses string stability as the uncertainty level reaches 20%; see Fig. 10(b-c).

For 20%-robust string stable case A, the speed profiles of human-driven vehicles 3 (red), 2 (green), 1 (purple) and the connected automated vehicle 0 (blue) are plotted in Fig. 12(a). While all vehicles have an average speed of about 22 [m/s], the severity of slow-downs for each vehicle can differ. Fig. 12(b) shows the response of human-driven and connected automated vehicles during one slow-down. While the minimum speed decreases from vehicle 3 to vehicle 1, indicating amplified speed perturbations, the connected automated vehicle is able to attenuate such a disturbance and maintains its speed well above 10 [m/s]. The amplification of speed variations by human drivers and attenuation by the connected automated vehicle can be further illustrated by the corresponding acceleration profiles. In Fig. 12(c), the peak deceleration of vehicle 1 (purple) reaches -8 [m/s²], while the deceleration of its predecessors (red and green) is no more than -6 [m/s²] and -5 [m/s²], respectively. Fig. 12(d) highlights such increasingly heavier deceleration from vehicle 3 to vehicle 1, while the connected automated vehicle maintains milder deceleration than the lead vehicle 3.

To further evaluate the acceleration/deceleration intensity of this 20%-robust string-stable design, we plot the normalized histograms (distributions) for the human-driven and connected

automated cars in Fig. 12(e-h). The occurrences of deceleration below -4 [m/s^2] can be observed to increase significantly from vehicle 3 to vehicle 1, which is corroborated by the standard deviation of the acceleration ($\text{std}(\dot{v}_3) = 1.286$ [m/s^2], $\text{std}(\dot{v}_2) = 1.235$ [m/s^2], $\text{std}(\dot{v}_1) = 1.592$ [m/s^2]). Based on this measure vehicle 2 slightly attenuates fluctuations, which could be an indicator for better driving skills. On the other hand, the least intense acceleration/deceleration is achieved by the connected automated vehicle, where the deceleration stays above -4 [m/s^2] and $\text{std}(\dot{v}_0) = 0.929$ [m/s^2]. The ratio $\text{std}(\dot{v}_0)/\text{std}(\dot{v}_3) \approx 0.722$ indicates that the 20%-robust string-stable CCC design significantly attenuates perturbations from the human-driven vehicles ahead.

However, a CCC design with less robustness may not be able to achieve the same level of attenuation. For case B, the velocity profiles are shown in Fig. 13(a-b), acceleration profiles in panels (c-d), and normalized acceleration distributions in panels (e-h). Similar observations can be made regarding the amplification of speed perturbations among human-driven vehicles. In order to compare the attenuation by the connected automated vehicle between cases A and B, we again compute the standard deviation of the accelerations, and obtain $\text{std}(\dot{v}_3) = 1.109$ [m/s^2], $\text{std}(\dot{v}_2) = 1.093$ [m/s^2], $\text{std}(\dot{v}_1) = 1.421$ [m/s^2], and $\text{std}(\dot{v}_0) = 0.906$ [m/s^2]. In this case the ratio $\text{std}(\dot{v}_0)/\text{std}(\dot{v}_3) \approx 0.817$, which is considerably larger than in case A. Furthermore, a direct comparison between Fig. 12(g,h) and Fig. 13(g,h) shows that the connected automated vehicle in case B is unable to maintain its deceleration above -4 [m/s^2] despite less frequent heavy braking of its immediate predecessor ($\dot{v}_1 < -6$ [m/s^2]).

Through the real-car experiments, we demonstrate that when exploiting motion data from multiple human-driven vehicles, a CCC design with higher levels of robustness performs better than a less robust design, even though both CCC designs perform significantly better than human drivers.

VI. CONCLUSION

In this paper, we applied structured singular value analysis to investigate the influences of uncertain human car-following parameters on string stability of connected cruise controllers. In particular, the uncertain time delays were considered using the Rekasius substitution, so that the robust bounds on head-to-tail string stability remained tight. We demonstrated through case studies that these robustness results could be used to design connected automated vehicles that reject traffic perturbations well despite uncertain human car-following behavior ahead.

Theoretical contributions were verified by experiments, that showed the advantage of robust control designs over classical methods. In measurements the robustly tuned control parameters were performing better under human-driver uncertainties than less robust control parameters.

Future research may include the robust stability analysis of parameter-varying and nonlinear systems in the presence of uncertainty.

ACKNOWLEDGMENT

The authors would like to thank the Commsignia, Inc. for the technical supports. They also acknowledge the help

of Sergei Avedisov, Sándor Beregi, Zsuzsanna Dobránszky, Chaozhe He, Ádám Kiss, Mehdi Sadeghpour, and Henrik Sykora during the experiments.

REFERENCES

- [1] P. Labuhn and W. J. Chundrlík, Jr., "Adaptive cruise control," U.S. Patent 5454442A, Oct. 3, 1995.
- [2] J. V. Werf, S. Shladover, M. Miller, and N. Kourjanskaia, "Effects of adaptive cruise control systems on highway traffic flow capacity," *Transp. Res. Rec., J. Transp. Res. Board*, vol. 1800, pp. 78–84, Jan. 2002. doi: [10.3141/1800-10](https://doi.org/10.3141/1800-10).
- [3] S. Shladover, D. Su, and X.-Y. Lu, "Impacts of cooperative adaptive cruise control on freeway traffic flow," *Transp. Res. Rec., J. Transp. Res. Board*, vol. 2324, no. 1, pp. 63–70, Jan. 2012. doi: [10.3141/2324-08](https://doi.org/10.3141/2324-08).
- [4] P. A. Barber, G. H. Engelman, P. J. King, and M. J. Richardson, "Adaptive cruise control system and methodology, including control of inter-vehicle spacing," EP Patent 1008482A2, Jun. 14, 2009.
- [5] V. Milanés, J. Alonso, L. Bouraoui, and J. Ploeg, "Cooperative maneuvering in close environments among cybercars and dual-mode cars," *IEEE Trans. Intell. Transp. Syst.*, vol. 12, no. 1, pp. 15–24, Mar. 2011.
- [6] M. Wang, W. Daamen, S. P. Hoogendoorn, and B. van Arem, "Rolling horizon control framework for driver assistance systems. Part II: Cooperative sensing and cooperative control," *Transp. Res. C, Emerg. Technol.*, vol. 40, pp. 290–311, Mar. 2014.
- [7] J. Ploeg, N. van de Wouw, and H. Nijmeijer, " \mathcal{L}_p string stability of cascaded systems: Application to vehicle platooning," *IEEE Trans. Control Syst. Technol.*, vol. 22, no. 2, pp. 786–793, Mar. 2014.
- [8] V. Milanés and S. E. Shladover, "Modeling cooperative and autonomous adaptive cruise control dynamic responses using experimental data," *Transp. Res. C, Emerg. Technol.*, vol. 48, pp. 285–300, Nov. 2014.
- [9] B. van Arem, C. J. G. van Driel, and R. Visser, "The impact of cooperative adaptive cruise control on traffic-flow characteristics," *IEEE Trans. Intell. Transp. Syst.*, vol. 7, no. 4, pp. 429–436, Dec. 2006.
- [10] J. Ploeg, D. P. Shukla, N. van de Wouw, and H. Nijmeijer, "Controller synthesis for string stability of vehicle platoons," *IEEE Trans. Intell. Transp. Syst.*, vol. 15, no. 2, pp. 854–865, Apr. 2014.
- [11] J. Lioris, R. Pedarsani, F. Y. Tascikaraoglu, and P. Varaiya, "Platoons of connected vehicles can double throughput in urban roads," *Transp. Res. C, Emerg. Technol.*, vol. 77, pp. 292–305, Apr. 2017.
- [12] S. E. Li, R. Li, J. Wang, X. Hu, B. Cheng, and K. Li, "Stabilizing periodic control of automated vehicle platoon with minimized fuel consumption," *IEEE Trans. Transport. Electrification*, vol. 3, no. 1, pp. 259–271, Mar. 2017.
- [13] E. van Nunen, M. R. J. A. E. Kwakkernaat, J. Ploeg, and B. D. Netten, "Cooperative competition for future mobility," *IEEE Trans. Intell. Transp. Syst.*, vol. 13, no. 3, pp. 1018–1025, Sep. 2012.
- [14] C. Englund *et al.*, "The grand cooperative driving challenge 2016: Boosting the introduction of cooperative automated vehicles," *IEEE Wireless Commun.*, vol. 23, no. 4, pp. 146–152, Aug. 2016.
- [15] S. E. Shladover, C. Nowakowski, X.-Y. Lu, and R. Ferlis, "Cooperative adaptive cruise control: Definitions and operating concepts," *Transp. Res. Rec., J. Transp. Res. Board*, vol. 2489, pp. 145–152, Dec. 2015. doi: [10.3141/2489-17](https://doi.org/10.3141/2489-17).
- [16] G. Orosz, "Connected cruise control: Modelling, delay effects, and nonlinear behaviour," *Vehicle Syst. Dyn.*, vol. 54, no. 8, pp. 1147–1176, Jun. 2016.
- [17] G. Orosz, J. I. Ge, C. R. He, S. S. Avedisov, W. B. Qin, and L. Zhang, "Seeing beyond the line of site—Controlling connected automated vehicles," *Mech. Eng. Mag.*, vol. 139, no. 12, pp. S8–S12, Dec. 2017.
- [18] L. Zhang and G. Orosz, "Motif-based design for connected vehicle systems in presence of heterogeneous connectivity structures and time delays," *IEEE Trans. Intell. Transp. Syst.*, vol. 17, no. 6, pp. 1638–1651, Jun. 2016.
- [19] J. I. Ge and G. Orosz, "Dynamics of connected vehicle systems with delayed acceleration feedback," *Transp. Res. C, Emerg. Technol.*, vol. 46, pp. 46–64, Sep. 2014.
- [20] S. S. Avedisov and G. Orosz, "Analysis of connected vehicle networks using network-based perturbation techniques," *Nonlinear Dyn.*, vol. 89, no. 3, pp. 1651–1672, Aug. 2017.
- [21] J. I. Ge, G. Orosz, D. Hajdu, T. Insperger, and J. Moehlis, "To delay or not to delay—Stability of connected cruise control," in *Time Delay Systems: Theory, Numerics, Applications and Experiments, Advances in Delays and Dynamics*, vol. 7. G. Orosz, T. Eersal, and T. Insperger, Eds. Springer, 2016, pp. 263–282. [Online]. Available: <https://www.springer.com/gp/book/9783319534251>

- [22] P. Seiler and R. Sengupta, "An H_{∞} approach to networked control," *IEEE Trans. Autom. Control*, vol. 50, no. 3, pp. 356–364, Mar. 2005.
- [23] J. P. Maschuw, G. C. Keßler, and D. Abel, "LMI-based control of vehicle platoons for robust longitudinal guidance," *IFAC Proc. Volumes*, vol. 41, no. 2, pp. 12111–12116, 2008.
- [24] S. E. Li, F. Gao, K. Li, L. Y. Wang, K. You, and D. Cao, "Robust longitudinal control of multi-vehicle systems—A distributed H -infinity method," *IEEE Trans. Intell. Transp. Syst.*, vol. 19, no. 9, pp. 2779–2788, Sep. 2018.
- [25] Y. Zheng, S. E. Li, K. Li, and W. Ren, "Platooning of connected vehicles with undirected topologies: Robustness analysis and distributed H -infinity controller synthesis," *IEEE Trans. Intell. Transp. Syst.*, vol. 19, no. 5, pp. 1353–1364, May 2018.
- [26] F. Gao, S. E. Li, Y. Zheng, and D. Kum, "Robust control of heterogeneous vehicular platoon with uncertain dynamics and communication delay," *IET Intell. Transp. Syst.*, vol. 10, no. 7, pp. 503–513, Sep. 2016.
- [27] A. Stotsky, C. C. Chien, and P. Ioannou, "Robust platoon-stable controller design for autonomous intelligent vehicles," in *Proc. 33rd IEEE Conf. Decis. Control*, Dec. 1994.
- [28] L. Zhang, J. Sun, and G. Orosz, "Hierarchical design of connected cruise control in the presence of information delays and uncertain vehicle dynamics," *IEEE Trans. Control Syst. Technol.*, vol. 26, no. 1, pp. 139–150, Jan. 2018.
- [29] M. di Bernardo, A. Salvi, and S. Santini, "Distributed consensus strategy for platooning of vehicles in the presence of time-varying heterogeneous communication delays," *IEEE Trans. Intell. Transp. Syst.*, vol. 16, no. 1, pp. 102–112, Feb. 2015.
- [30] W. B. Qin and G. Orosz, "Scalable stability analysis on large connected vehicle systems subject to stochastic communication delays," *Transp. Res. C, Emerg. Technol.*, vol. 83, pp. 39–60, Oct. 2017.
- [31] Y. Zhou, S. Ahn, M. Chitturi, and D. A. Noyce, "Rolling horizon stochastic optimal control strategy for ACC and CACC under uncertainty," *Transp. Res. C, Emerg. Technol.*, vol. 83, pp. 61–76, Oct. 2017.
- [32] B. Besselink and K. H. Johansson, "String stability and a delay-based spacing policy for vehicle platoons subject to disturbances," *IEEE Trans. Autom. Control*, vol. 62, no. 9, pp. 4376–4391, Sep. 2017.
- [33] J. C. Doyle, "Analysis of feedback systems with structured uncertainties," *IEE Proc. D-Control Theory Appl.*, vol. 129, no. 6, pp. 242–250, Nov. 1982.
- [34] K. Zhou and J. C. Doyle, *Essentials Robust Control* (Prentice Hall Modular Series for Eng). Upper Saddle River, NJ, USA: Prentice-Hall, 1998.
- [35] J. I. Ge and G. Orosz, "Dynamics of connected vehicle systems with delayed acceleration feedback," *Transp. Res. C, Emerg. Technol.*, vol. 46, pp. 46–64, Sep. 2014.
- [36] J. I. Ge, S. S. Avedisov, C. R. He, W. B. Qin, M. Sadeghpour, and G. Orosz, "Experimental validation of connected automated vehicle design among human-driven vehicles," *Transp. Res. C, Emerg. Technol.*, vol. 91, pp. 335–352, Jun. 2018.
- [37] J. I. Ge and G. Orosz, "Connected cruise control among human-driven vehicles: Experiment-based parameter estimation and optimal control design," *Transp. Res. C, Emerg. Technol.*, vol. 95, pp. 445–459, Oct. 2018.
- [38] A. Salvi, S. Santini, and A. S. Valente, "Design, analysis and performance evaluation of a third order distributed protocol for platooning in the presence of time-varying delays and switching topologies," *Transp. Res. C, Emerg. Technol.*, vol. 80, pp. 360–383, Jul. 2017.
- [39] Y. Zheng, S. E. Li, J. Wang, L. Y. Wang, and K. Li, "Stability and scalability of homogeneous vehicular platoon: Study on the influence of information flow topologies," *IEEE Trans. Intell. Transp. Syst.*, vol. 17, no. 1, pp. 14–26, Jan. 2016.
- [40] N. Bekiaris-Liberis, C. Roncoli, and M. Papageorgiou, "Predictor-based adaptive cruise control design," *IEEE Trans. Intell. Transp. Syst.*, vol. 19, no. 10, pp. 3181–3195, Oct. 2018.
- [41] T. G. Molnár, W. B. Qin, T. Insperger, and G. Orosz, "Application of predictor feedback to compensate time delays in connected cruise control," *IEEE Trans. Intell. Transp. Syst.*, vol. 19, no. 2, pp. 545–559, Feb. 2018.
- [42] D. Helbing, "Traffic and related self-driven many-particle systems," *Rev. Mod. Phys.*, vol. 73, no. 4, pp. 1067–1141, Oct. 2001.
- [43] P. Seiler, A. Pant, and K. Hedrick, "Disturbance propagation in vehicle strings," *IEEE Trans. Autom. Control*, vol. 49, no. 10, pp. 1835–1841, Oct. 2004.
- [44] D. Hinrichsen and A. J. Pritchard, *Mathematical Systems Theory I: Modelling, State Space Analysis, Stability and Robustness* (Texts in Applied Mathematics). Berlin, Germany: Springer, 2006.
- [45] C. Scherer, "Theory of robust control," Mech. Eng. Syst. Control Group, Delft Univ. Technol., Delft, The Netherlands, Course Notes, 2001.
- [46] P. M. Young, M. P. Newlin, and J. C. Doyle, " μ analysis with real parametric uncertainty," in *Proc. 30th IEEE Conf. Decis. Control*, Dec. 1991, pp. 1251–1256.
- [47] A. Packard and J. Doyle, "The complex structured singular value," *Automatica*, vol. 29, no. 1, pp. 71–109, Jan. 1993.
- [48] M. K. H. Fan, A. L. Tits, and J. C. Doyle, "Robustness in the presence of mixed parametric uncertainty and unmodeled dynamics," *IEEE Trans. Autom. Control*, vol. 36, no. 1, pp. 25–38, Jan. 1991.
- [49] G. J. Balas, J. C. Doyle, K. Glover, A. Packard, and R. Smith, *μ -Analysis and Synthesis Toolbox for Use with MATLAB: User's Guide*. Natick, MA, USA: The MathWorks, 1993.
- [50] N. Olgac and R. Sipahi, "An exact method for the stability analysis of time-delayed linear time-invariant (LTI) systems," *IEEE Trans. Autom. Control*, vol. 47, no. 5, pp. 793–797, May 2002.
- [51] Z.-Q. Wang and P. Lundström, and S. Skogestad, "Representation of uncertain time delays in the H_{∞} framework," *Int. J. Control*, vol. 59, no. 3, pp. 627–638, Mar. 1994.
- [52] D. Bachrathy and G. Stépán, "Bisection method in higher dimensions and the efficiency number," *Mech. Eng.*, vol. 56, no. 2, pp. 81–86, 2012.
- [53] *Dedicated Short Range Communications (DSRC) Message Set Dictionary Set*, Standard SAE J2735SET_201603, 2016.



Dávid Hajdu received the B.Sc. degree in mechatronics engineering and the M.Sc. degree in mechanical engineering modeling from the Budapest University of Technology and Economics in 2013 and 2015, respectively, where he is currently pursuing the Ph.D. degree with the Department of Applied Mechanics.



Jin I. Ge received the bachelor's degree in transportation engineering and the master's degree in automotive engineering from the Beijing University of Aeronautics and Astronautics in 2010 and 2012, respectively, and the Ph.D. degree in mechanical engineering from the University of Michigan, Ann Arbor, MI, USA, in 2017. She was a Post-Doctoral Researcher with the California Institute of Technology from 2017 to 2018. She is currently a Research Scientist with the Toyota Research Institute. Her research interests include dynamics and control, formal verification, and time delay systems.



Tamás Insperger received the M.Sc. and Ph.D. degrees in mechanical engineering from the Budapest University of Technology and Economics (BME) in 1999 and 2002, respectively, and the D.Sc. degree from the Hungarian Academy of Sciences (MTA) in 2015. He became an Assistant Professor, an Associate Professor, and a Professor with the Department of Applied Mechanics, BME, in 2003, 2008, and 2018, respectively. In 2016, he has become the Leader of the MTA-BME Lendület Human Balancing Research Group. He has been

the Head of the Department of Applied Mechanics since 2018. His current research interests include nonlinear dynamics, control and time delay systems with applications on machine tool vibrations, human controlled systems, and human balancing.



Gábor Orosz received the M.Sc. degree in engineering physics from the Budapest University of Technology in 2002 and the Ph.D. degree in engineering mathematics from the University of Bristol in 2006. He held a post-doctoral position with the University of Exeter and the University of California at Santa Barbara, Santa Barbara, CA, USA. In 2010, he joined the University of Michigan, Ann Arbor, MI, USA, where he is currently an Associate Professor in mechanical engineering. His research interests include nonlinear dynamics and control, time delay

systems, and networks and complex systems with applications on connected and automated vehicles.